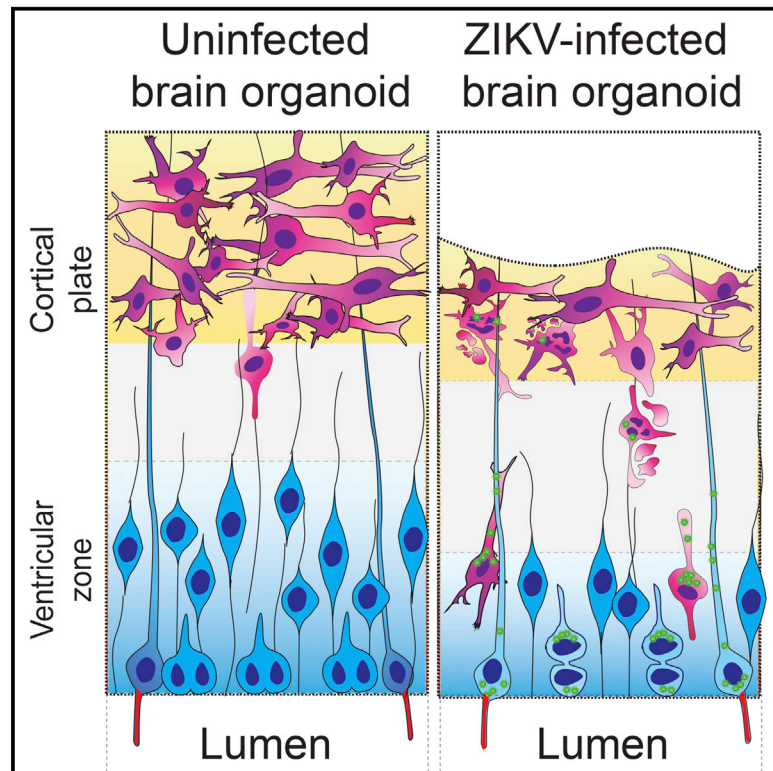# Cell Stem Cell

Recent Zika Virus Isolates Induce Premature Differentiation of Neural Progenitors in Human Brain Organoids

Graphical Abstract

Authors

Elke Gabriel, Anand Ramani, Ulrike Karow, ..., Martin Krönke, Olaf Utermöhlen, Jay Gopalakrishnan

Correspondence

jay.gopalakrishnan@uni-koeln.de

In Brief

Gabriel and colleagues show that two recently isolated Zika strains efficiently infect neural progenitors in human brain organoids and cause premature differentiation in a way that closely resembles Zika-associated microcephaly and differs from the effects seen with an older and extensively passaged strain.

Highlights

- Recent American/Asian ZIKV isolates readily infect human iPSC-derived brain organoids

- Infection triggers premature differentiation of NPCs, leading to progenitor depletion

- Infected NPCs show centrosome disruption and alterations in division plane

- NPC depletion leads to cortical thinning resembling ZIKV-associated microcephaly

CellPress

Recent Zika Virus Isolates Induce Premature Differentiation of Neural Progenitors in Human Brain Organoids

Elke Gabriel,[1] Anand Ramani,[1] Ulrike Karow,[2] Marco Gottardo,[3] Karthick Natarajan,[1] Li Ming Gooi,[1]
Gladiola Goranci-Buzhala,[1] Oleg Krut,[2] Franziska Peters,[4] Milos Nikolic,[5] Suvi Kuivanen,[6] Essi Korhonen,[6] Teemu Smura,[6]
Olli Vapalahti,[6,7] Argyris Papantonis,[5] Jonas Schmidt-Chanasit,[8,9] Maria Riparbelli,[3] Giuliano Callaini,[3]
Martin Krönke,[2,5,9,10] Olaf Utermöhlen,[2,5] and Jay Gopalakrishnan[1,11,*]

[1]Center for Molecular Medicine and Institute of Biochemistry I of the University of Cologne, Cologne 50931, Germany
[2]Institute for Medical Microbiology, Immunology, and Hygiene, University of Cologne, Cologne 50935, Germany
[3]Department of Life Sciences, University of Siena, Siena 53100, Italy
[4]Department of Dermatology, University of Cologne, Cologne 50931, Germany
[5]Center for Molecular Medicine of the University of Cologne, Cologne 50931, Germany
[6]Department of Virology, Helsinki University Hospital, Helsinki 00029, Finland
[7]Department of Veterinary Biosciences, University of Helsinki, Helsinki 00029, Finland
[8]Bernhard Nocht Institute for Tropical Medicine, Hamburg 20359, Germany
[9]German Center for Infection Research (DZIF), Bonn-Cologne, Cologne 50935, Germany
[10]CECAD, Cologne, Germany
[11]Lead Contact
*Correspondence: jay.gopalakrishnan@uni-koeln.de
http://dx.doi.org/10.1016/j.stem.2016.12.005

SUMMARY

The recent Zika virus (ZIKV) epidemic is associated with microcephaly in newborns. Although the connection between ZIKV and neurodevelopmental defects is widely recognized, the underlying mechanisms are poorly understood. Here we show that two recently isolated strains of ZIKV, an American strain from an infected fetal brain (FB-GWUH-2016) and a closely-related Asian strain (H/PF/2013), productively infect human iPSC-derived brain organoids. Both of these strains readily target to and replicate in proliferating ventricular zone (VZ) apical progenitors. The main phenotypic effect was premature differentiation of neural progenitors associated with centrosome perturbation, even during early stages of infection, leading to progenitor depletion, disruption of the VZ, impaired neurogenesis, and cortical thinning. The infection pattern and cellular outcome differ from those seen with the extensively passaged ZIKV strain MR766. The structural changes we see after infection with these more recently isolated viral strains closely resemble those seen in ZIKV-associated microcephaly.
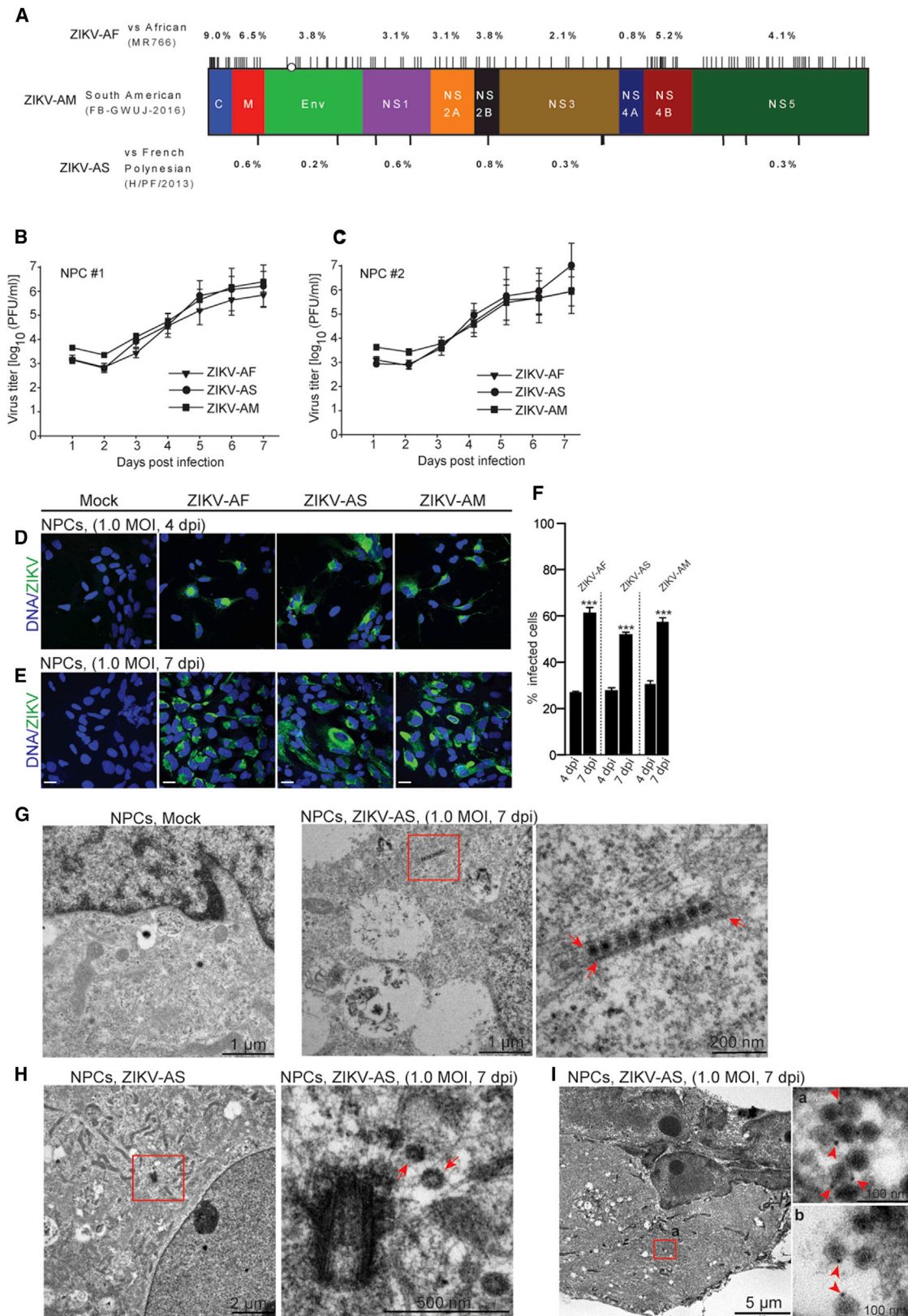
INTRODUCTION

The Zika virus (ZIKV) epidemic in the Americas coincided with a sudden increase of microcephaly-associated cases. Detection of ZIKV in the amniotic fluid of infected pregnant women and microcephalic fetal brain tissues linked ZIKV to microcephaly

(Brasil et al., 2016; Calvet et al., 2016; Driggers et al., 2016; Mlakar et al., 2016; Ventura et al., 2016).

Recent studies have elucidated neurotropism for ZIKV strains, including the prototypic African MR766 strain (ZIKV-AF), which has been extensively passaged since it was first isolated from non-human sentinel primates in 1947 (Cugola et al., 2016; Dang et al., 2016; Dick et al., 1952; Garcez et al., 2016; Qian et al., 2016; Tang et al., 2016). These studies, using ZIKV-AF to infect neural progenitor cells (NPCs), suggest that ZIKV infection induces strong apoptotic cell death, which affects neurogenesis.

Here we functionally characterize the low-passage recent outbreak ZIKV strains H/PF/2013 (ZIKV-AS) and FB-GWUH-2016 (ZIKV-AM) (Driggers et al., 2016; Hamel et al., 2015). ZIKV-AM was isolated from an infected fetal brain with neurologic abnormalities. We also used the extensively passaged ZIKV-AF because it was used in many recent studies. ZIKV-AS and -AM are phylogenetically more closely related to each other compared with ZIKV-AF (Figure 1A). To model ZIKV infection in the developing human brain, we used recently described human induced pluripotent stem cell (iPSC)-derived brain organoids that recapitulate early neurodevelopmental events (Gabriel et al., 2016; Lancaster et al., 2013; Mariani et al., 2015).

In 2D neural cultures, all three ZIKV strains productively infected NPCs, consistent with previous reports (Cugola et al., 2016; Dang et al., 2016; Tang et al., 2016). In 3D brain organoids, ZIKV-AS/AM readily infect proliferating ciliated apical neural progenitors of the ventricular zone (VZ) soon after infection. ZIKV infection perturbs centrosomal structures of NPCs and leads to an altered division plane of mitotic apical neural progenitors in organoids. This is accompanied by premature differentiation of NPCs, leading to progenitor depletion and impairment of neurogenesis. The infection pattern of ZIKV-AS and ZIKV-AM

Figure 1. Productive Infection of NPCs by ZIKV Strains

(A) Differences in the polyprotein of ZIKV-AF (top) in comparison with ZIKV-AM (center) and ZIKV-AS (bottom). Vertical lines, amino acid exchanges; circle, deletion.

and cellular responses differ from those seen with ZIKV-AF. Together, our results, revealing NPC depletion, impairment of neurogenesis, and structural changes induced by recent isolates in human brain organoids, provide possible mechanisms for ZIKV causing brain malformations.

RESULTS

ZIKV Strains Productively Infect NPCs

We infected NPCs derived from two different iPSC lines with ZIKV strains. Infection with any of the three strains produced similar amounts of viral progeny (Figures 1B and 1C). The intracellular detection of ZIKV envelope protein at a low MOI further indicated productive infection (Figures 1D and 1E). Infection rates increased from 30% to 60% within 4–7 days post-infection (dpi) (Figure 1F). Furthermore, intracellular viral particles in infected NPCs were detected by transmission electron microscopy (TEM) as electron-dense spheres of ~60-nm diameter (56.3 ± 3 nm; Table S1) in the vicinity of actin filaments, centrioles, and microtubules (Figures 1G and 1H; Figures S1A–S1C). Immunogold labeling confirmed the viral identity of these electron-dense spheres (Figure 1I). These data indicate that infection rates and viral progeny production for all three ZIKV strains are similar.

ZIKV Strains Trigger Premature Differentiation of NPCs

Self-renewing, multipotent NPCs can give rise to almost any cell type of the developing brain. NPC differentiation into neuronal lineages is termed neurogenesis (Götz and Huttner, 2005). Neural epithelium development requires initial symmetric division of NPCs to reach an ample pool before switching to asymmetric division to generate cells that form different cortical layers (Alcantara and O'Driscoll, 2014; Calegari and Huttner, 2003; Götz and Huttner, 2005). Disturbances of cell division are prone to diminish the proportion of symmetric divisions, leading to NPC pool depletion and reduction of neurons generated. Analyzing brain organoids derived from microcephaly patients of genetic origin identified premature differentiation of NPCs as a potential cause for the observed phenotypes (Alcantara and O'Driscoll, 2014; Gabriel et al., 2016; Lancaster et al., 2013).

ZIKV infection reduced NPC proliferation, which is consistent with a recent report that ZIKV infection attenuates NPC proliferation in the adult mouse brain (Figure 2A; Li et al., 2016). A delay in the cell cycle, leading to reduced proliferation, is associated with NPC differentiation (Gabriel et al., 2016; Lancaster et al., 2013). The strongest reduction in NPC proliferation was observed with ZIKV-AF (Figure 2A). However, when we tested whether ZIKV infection triggers NPC differentiation into neurons under non-differentiation conditions, we noticed that ZIKV-AF induced significantly less differentiation than ZIKV-AS/AM by 4

dpi. ZIKV-AS/AM induced NPC differentiation into TUJ1-positive neurons at higher frequencies (Figures 2B and 2C; magenta bars in Figure 2C). ZIKV localized to the perinuclear space of differentiated TUJ1-positive neurons, further supporting that ZIKV-infection could induce NPC differentiation (Figure 2D). Assuming ongoing differentiation, we expected an accumulation of TUJ1-positive neurons induced by ZIKV-AS/AM at 7 dpi. However, by 7 dpi, compared with 4 dpi, TUJ1-positive neurons did not accumulate but, rather, remained at about the same frequency in cultures infected with ZIKV-AS/AM. These findings indirectly suggest that differentiated TUJ1-positive neurons might undergo cell death, corresponding with the observation of increased apoptotic cells at 7 dpi in ZIKV-AS- and ZIKV-AM-infected cultures (Figure 2C, black bars). In ZIKV-AF-infected cultures, we noticed the highest proportion of apoptotic cells coinciding with a significant reduction of nestin-positive cells by 7 dpi (Figure 2C, green bars). These results suggest that ZIKV-AM and AS reduces NPCs proliferation, triggers differentiation, and induces some apoptosis.

ZIKV Infection Perturbs Centrosomal Structures of NPCs

Defective centrosomes because of poor recruitment of centrosomal proteins are a hallmark of prematurely differentiating NPCs in microcephaly (Gabriel et al., 2016; Lancaster et al., 2013; Zheng et al., 2014). Indeed, ZIKV infection reduces the centrosomal recruitment of the microcephaly-linked proteins Cep152, PCNT, and CPAP (Figures 3A–3D; Bond et al., 2005; Cizmecioglu et al., 2010; Guernsey et al., 2010; Rauch et al., 2008).

ZIKV-infected interphase NPCs also exhibited reduced levels of CEP164, which localizes to mother centriole appendages for ciliogenesis (Graser et al., 2007). Serial sectioning EM analyses revealed that mother centrioles lack appendages and one of the triplet microtubular blades at their distal ends (Figure 3Ei and ii; Figures S1D–S1E). Such structurally damaged centrosomes of interphase cells could potentially give rise to multiple centrosomal structures during mitosis, as recently reported (Onorati et al., 2016). Together, these effects of ZIKV infection on centrosomal structures are reminiscent of centrosomal defects found in cells derived from patients with genetically caused microcephaly (Gabriel et al., 2016; Hussain et al., 2012; Kalay et al., 2011; Lancaster et al., 2013).

ZIKV Strains Productively Infect iPSC-Derived Human Brain Organoids and Display Distinct Localization Patterns

To test whether ZIKV infection could lead to microcephaly-like phenotypes in 3D brain organoids, we infected human brain

(B and C) ZIKV-AF/AS/AM virus titers from two independent NPCs supernatants. Shown are titer values after infection with MOI 1.0, determined as plaque forming units (PFUs)/mL on Vero cells. Error bars show mean ± SEM; n = 3 independent experiments.

(D and E) ZIKV-infected NPCs (green) after 4 and 7 dpi. Scale bar, 5 μm.

(F) Percentages of ZIKV-AF/AS/AM-infected NPCs at 4 and 7 dpi. Data are ± SEM. ***p < 0.001, ordinary one-way ANOVA; n = 3 independent experiments from two different NPC lines. More than 400 cells were analyzed under each condition.

(G) EM shows virus-like particles within ZIKV-AS-infected NPCs. Arrows at the right show particles with an actin filament-like structure. See also Figures S1A–S1C.

(H) Virus-like particles in the vicinity of a centriole structure. More than 30 ZIKV-AS-infected NPCs were analyzed. See also Table S1.

(I) 5-nm immunogolds (arrowheads) at the surfaces of spheres, confirming that they are flaviviral particles (a). (b) is a second example from a different cell.
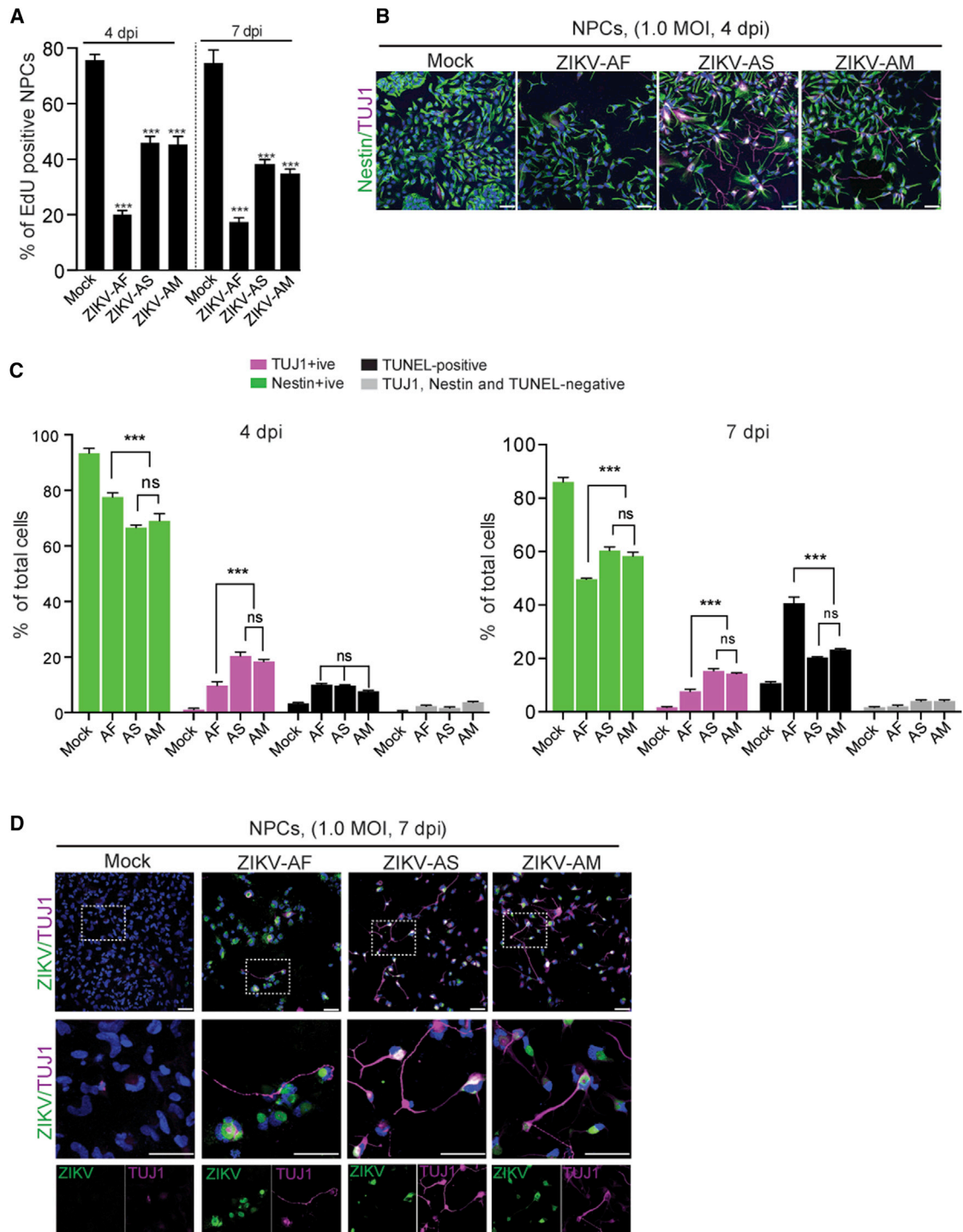
Figure 2. ZIKV Infection Causes NPCs Differentiation

(A) ZIKV infection reduces 5-ethynyl-2′-deoxyuridine (EdU) incorporation after 24-hr pulse-chasing. EdU-positive cells were scored among nestin-positive NPCs. Data are ± SEM. ***p < 0.001, one-way ANOVA, followed by Tukey's multiple comparisons test. n = 3 independent experiments from two different NPC lines. More than 400 cells were analyzed under each condition.

(B) ZIKV-infected NPCs (green) differentiated into TUJ1-positive neurons (magenta) at 4 dpi. Mock or UV irradiation ZIKV treatment did not have any effect. Scale bar, 5 μm.

(C) Percentages of nestin-containing (green), TUJ1-containing (magenta), and TUNEL-containing (black) cells and cells containing no marker (gray) in ZIKV-AF/AS/AM-infected NPC cultures at 4 and 7 dpi. Although the percentages of TUNEL-positive cells are similar in infected cultures, NPC differentiation into TUJ1-positive neurons induced by ZIKV-AS/AM strains is significantly higher than that induced by ZIKV-AF (magenta bars). By 7 dpi, compared with 4 dpi, the

(legend continued on next page)

organoids. ZIKV strains productively infected human 3D brain organoids derived from two independent iPSC lines (Figures 4A and 4B). Electron microscopy (EM) analysis further confirmed the intracellular localization of ZIKV-AS particles (Figure S1F). We infected 9-day-old organoids and cultured them further for 2, 5, and 11 days prior to analysis. Although uninfected organoids grew up to 3 mm in size, ZIKV-infected organoids exhibited attenuated growth (Figure 4C).

A typical VZ of a brain organoid contains nestin-, SOX2-, and PAX6-positive proliferating radial glial cells at the apical side facing the lumen and TUJ1-, DCX-, and MAP2-positive neurons forming a primitive cortical region at the basal side spatially distinct from the lumen and VZ (Gabriel et al., 2016; Lancaster et al., 2013; Mariani et al., 2015) (Figure 4D; Figures S2A–S2D).

While analyzing the kinetics of ZIKV infection, we noticed that ZIKV-AS/AM readily targeted to proliferating apical progenitors of the VZ on day 2 (Figure 4Di; Figures S2A and S2B). Apical progenitors protrude Arl13b-positive primary cilia from their apical surface into the lumen of the VZ, where AXL, a candidate ZIKV entry receptor, is localized (Figures S2E–S2G; Nowakowski et al., 2016). ZIKV localized to radial filament-like structures between the progenitors, suggesting that ZIKV can also target radial processes emerging from the VZ (Figure 4D).

On day 2, ZIKV-AF localized to the surface of the organoid distinct from the VZ (Figures 4Di and 4Ei; Figures S2A and S2B). This localization of ZIKV-AF at the region corresponding to the primitive cortical region is consistent with a recent report of ZIKV-AF targeting immature neurons, intermediate progenitors, and astrocytes at the surface of organoids (Qian et al., 2016). On subsequent days of infection, frequencies of ZIKV-AS/AM-positive cells were increased at the VZ (Figures 4D and 4E). Together, ZIKV-AS/AM isolates largely localize to apical progenitors of the VZ.

ZIKV-AM and AS Cause Limited Cell Death of Progenitors at the VZ

ZIKV-AS/AM present in cells at the VZ exhibiting typical radial glial morphology even at 11 dpi suggests that the viability of these cells is not considerably affected. In contrast, we detected terminal deoxynucleotidyl transferase dUTP nick end labeling (TUNEL)-positive apoptotic cells in areas distinct from the VZ where TUJ1-positive neurons accumulate (Figures S3A–S3D). We scored apoptotic cells by the TUNEL assay because activated caspase-3 is upregulated during NPC differentiation independently from cell death (D'Amelio et al., 2010; Fernando et al., 2005). This suggests that ZIKV infection could induce the death of differentiated neuronal cells emerging from the VZ to form the primitive cortical plate. Concurrently, TUJ1-, MAP2-, and DCX-positive regions were reduced at the surface of organoids (Figures S2C and S2D).

To directly test whether ZIKV-infection could induce neuronal cell death, we infected cortical neurons differentiated from two

NPC lines (Paşca et al., 2015). ZIKV infection rates reached up to 40%, coinciding with cell death after 6 days of infection (Figures S3E–S3H). Thus, the defective cortical region in ZIKV-infected organoids is reminiscent of the neurodevelopmental defects in microcephaly.

Although ZIKV-AS/AM do not seem to majorly affect the viability of apical progenitors, the presence of viral antigen suggests replication in these cells (Figure 4D; Figures S2A, S2B, and S2E–S2G). However, these strains cause apoptosis of neurons on later days of infection (Figures S3A–S3D). Early after infection, ZIKV-AF localizes to the organoid surface and spreads deeper into organoids at later time points. This coincides with an increase in overall TUNEL-positive cells, accompanied by disruption of the cyto-architecture of organoids (Figure 4Diii; Figures S3A–S3D and S4A–S4D). On day 11 dpi, ZIKV-AS/AM-infected organoids exhibited thinner VZs than uninfected organoids, possibly caused by NPC loss because of premature differentiation (Figure S3I; Figures 2B and 2C). To assess whether this effect is specific for ZIKV, we infected organoids with the unrelated lymphocytic choriomeningitis virus (LCMV) strain WE as a control. Although LCMV-WE causes productive infection of organoids, it neither reduced organoid growth nor the thickness of VZs, suggesting that VZ thinning is specific for ZIKV infection (Figures S4E–S4G).

ZIKV-Infected Organoids Display an Altered Division Plane of Mitotic Apical Progenitors

To address the kinetics of NPC differentiation induced by ZIKV strains, we analyzed the division plane of phospho-vimentin-positive apical neural progenitors of the VZ (see the STAR Methods). A horizontally oriented division plane is essential for early symmetric expansion of NPCs (Rakic, 1995; Yingling et al., 2008). When neurogenesis begins after sufficient NPC expansion, the dividing cells change their orientation toward the lumen, and the division plane switches from horizontal to vertical (Gabriel et al., 2016; Lancaster et al., 2013; Rakic, 1995). Cell cycle delay leading to premature differentiation has been shown to be accompanied by increased proportions of vertically oriented NPCs (Calegari et al., 2005; Gabriel et al., 2016; Tapias et al., 2014). In contrast to VZs in uninfected organoids, ZIKV-infected VZs displayed increased frequencies of vertically oriented mitotic progenitors, indicating unscheduled switching of the division plane (Figures 4F–4H). This could contribute to premature differentiation with concomitant depletion of progenitors. This was paralleled by the decline of total mitotic apical progenitors in ZIKV-infected organoids and the occasional observation of TUJ1-positive differentiated cells in the vicinity of the lumen, a region usually containing proliferating apical progenitors (Figure 4I; Figures S4H and S4I). These findings are in agreement with premature differentiation caused by impaired centrosome function (Bazzi and Anderson, 2014; Gabriel et al., 2016; Garcez et al., 2015; Insolera et al., 2014).

---

frequencies of TUJ1-positive neurons remained the same. ZIKV-AF induces higher apoptosis. In ZIKV-AF-infected NPCs, at 7 dpi, the apoptotic cell number is significantly higher (black bars), and the percentages of the nestin-positive (green) and TUJ1-positive (magenta) cell portion are significantly less than that observed in ZIKV-AS/AM-infected cultures. n = 4 independent experiments from two different NPC lines. Data are ± SEM. ***p < 0.001, two-way ANOVA. At least 200 cells were analyzed under each condition in multiple microscopic fields.

(D) ZIKV-AF/AS/AM-infected NPCs spontaneously differentiate into TUJ1-positive neurons (magenta). Center: perinuclear space ZIKV localization (green) in differentiated neurons (magenta). Scale bars, 5 μm (top) and 10 μm (center).
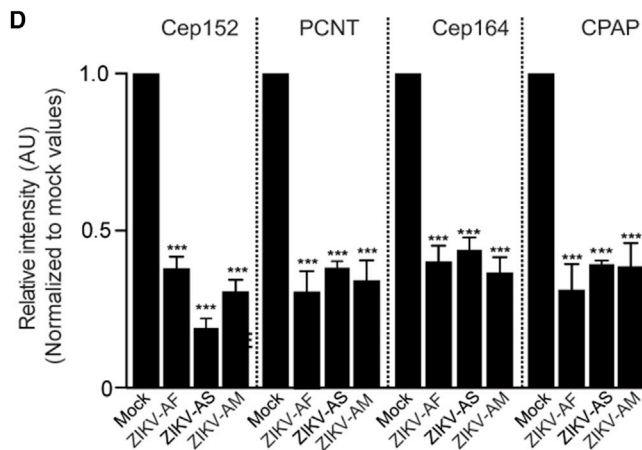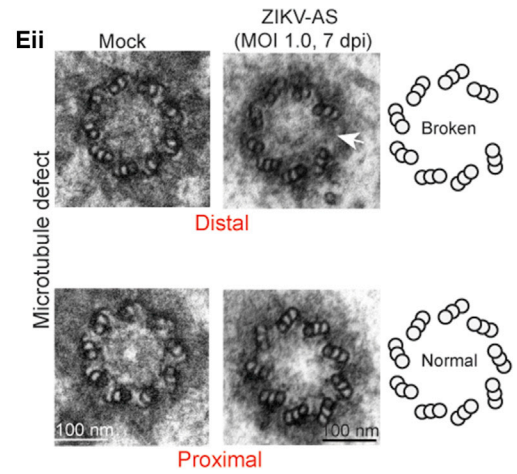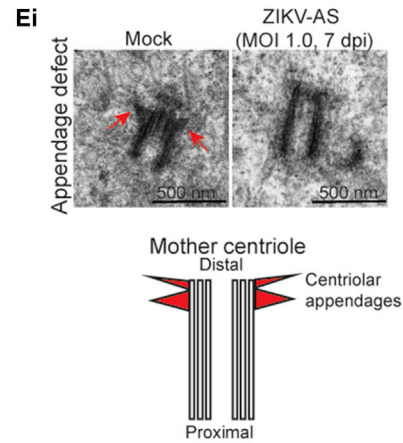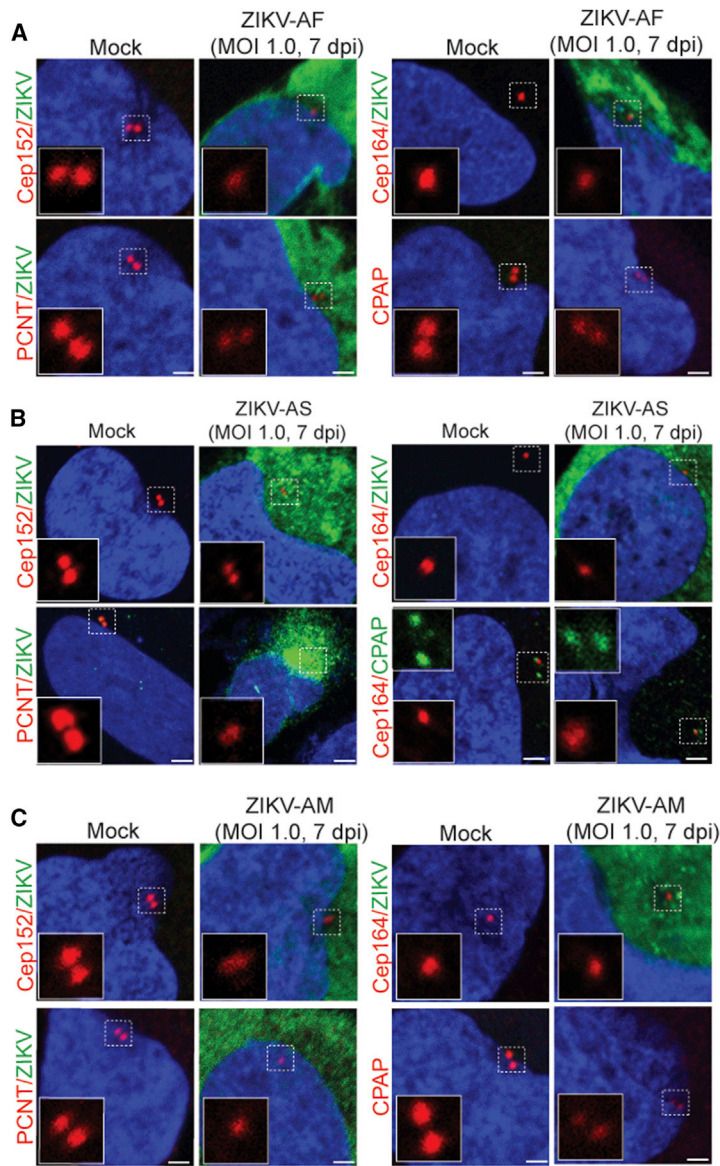
(legend on next page)

DISCUSSION

In this work, we analyzed low-passage American and Asian ZIKV strains from recent outbreaks in 2D neural cultures and 3D human brain organoids. ZIKV-AM and AS readily target proliferating apical progenitors in 3D brain organoids. Concurrently, ZIKV-AM and AS trigger premature differentiation of NPCs at early phases of infection, leading to depletion of progenitors. Interestingly, proliferating progenitors of the VZ targeted by ZIKV-AS/AM are less prone to die. Indeed, at early stages of infection, flaviviruses can protect infected cells from death for viral replication (Brault et al., 2016; McLean et al., 2011).

The reasons for the vulnerability of the developing brain to ZIKV infection remain largely unknown. It also remains to be explored whether there are common mechanisms between acquired microcephaly because of ZIKV infection and inherited microcephaly because of genetic mutations in centrosomal genes. During early embryonic brain development, self-renewing multipotent NPCs undergo rapid symmetric division, requiring an error-free cell division program. Centrosomes are essential for accurate cell division. Thus, any aberrant centrosomal function can impair initial symmetric divisions during early brain development. This could cause premature NPC differentiation, ultimately leading to NPC pool depletion, as observed in microcephaly of genetic origin (Gabriel et al., 2016; Lancaster et al., 2013).

In ZIKV-infected NPCs, we observed centrosomal structural defects, including impaired recruitment of centrosomal proteins (Figure 3). Additionally, we observed defects in the symmetric division of NPCs at the VZ, where ZIKV replication occurs (Figures 4F–4I). Similar alterations were reported for genetically caused microcephaly (Gabriel et al., 2016; Hussain et al., 2012; Kalay et al., 2011; Lancaster et al., 2013; Zheng et al., 2014).

In summary, our findings link contemporary ZIKV strains and microcephaly in a disease-relevant experimental system. Specifically, recent outbreak ZIKV strains tend to induce subtle damage, such as premature differentiation of NPCs, leading to depletion of the NPC pool. The resulting insufficiency in the NPC pool could then potentially impair the cellularity of brain development and the structural organization of the primitive cortical plate in a developing brain, a hallmark of microcephaly.

STAR★METHODS

Detailed methods are provided in the online version of this paper and include the following:

- KEY RESOURCES TABLE
- CONTACT FOR REAGENT AND RESCOURCE SHARING
- EXPERIMENTAL MODEL AND SUBJECT DETAILS

  - ZIKV and LCMV-WE strains
  - Human iPSCs
  - iPSC-derived NPCs, brain organoids and Neurons
- METHOD DETAILS
  - ZIKV counting
  - Virus infection
  - Mock treatment
  - Differentiation of iPSCs into NPCs
  - NPC culture and infection
  - Generation of brain organoids
  - Infection of brain organoids
  - Infection of neurons
  - Fixation of NPCs and neurons
  - Fixation and cryosectioning of organoids
  - Permeabilization, antigen retrieval and blocking
  - Immunofluorescent staining
  - TUNEL assay
  - EdU pulse labeling assay
  - Determination of division plane in aRGs
  - Transmission electron microscopy
  - Immuno electron microscopy
  - Image acquisition
  - ZIKV protein sequence alignment
- QUANTIFICATION AND STATISTICAL ANALYSIS

SUPPLEMENTAL INFORMATION

Supplemental Information includes four figures and two tables and can be found with this article online at http://dx.doi.org/10.1016/j.stem.2016.12.005.

AUTHOR CONTRIBUTIONS

Conceptualization, E.G., O.U., M.K., and J.G.; Methodology, E.G, O.U., M.K., and J.G.; Investigation, E.G. and A.R.; Formal Analysis, O.K.; Investigation (Molecular Biology, Imaging and Bioinformatics), K.N., L.M.G., G.G.B., A.P., and M.N.; Investigation (Virus Cultivation and Infection), U.K., F.P., and O.U.; Resources, S.K., E.K., T.S., J.S.C., and O.V.; Investigation (EM), M.G., M.R., and G.C.; Writing – Original Draft, E.G., O.U., M.K., and J.G.; Writing – Review & Editing, E.G., O.U., M.K., and J.G.; Supervision, O.U. and J.G.; Funding Acquisition, O.U., M.K., and J.G. All authors analyzed the data and contributed to manuscript preparation.

Figure 3. ZIKV Infection Perturbs Centrosomes of NPCs

(A–C) Centrosomes of ZIKV-AF-infected (A), ZIKV-AS-infected (B), and ZIKV-AM-infected (C) NPCs fail to efficiently recruit Cep152, PCNT, Cep164, and CPAP. Scale bar, 1 μm.

(D) Relative protein intensities normalized to mock values. Data are ± SEM. ***p < 0.001, Student's t test. n = 3 independent experiments from two different NPC lines. More than 100 cells were analyzed under each condition.

(E) i: EM shows a normal centriole with centriolar appendages (arrows, mock) and appendage defect in ZIKV-AS-infected NPC. A schematic of a mother centriole with appendages is shown below. More than 20 cells were analyzed under each condition. ii: Cross section of a centriole in mock- and ZIKV-AS-infected NPCs. ZIKV-AS-infected cells lack one of the triplet microtubular blades at their distal end (white arrow). More than 20 cells were analyzed under each condition.
See also Figures S1D and S1E.
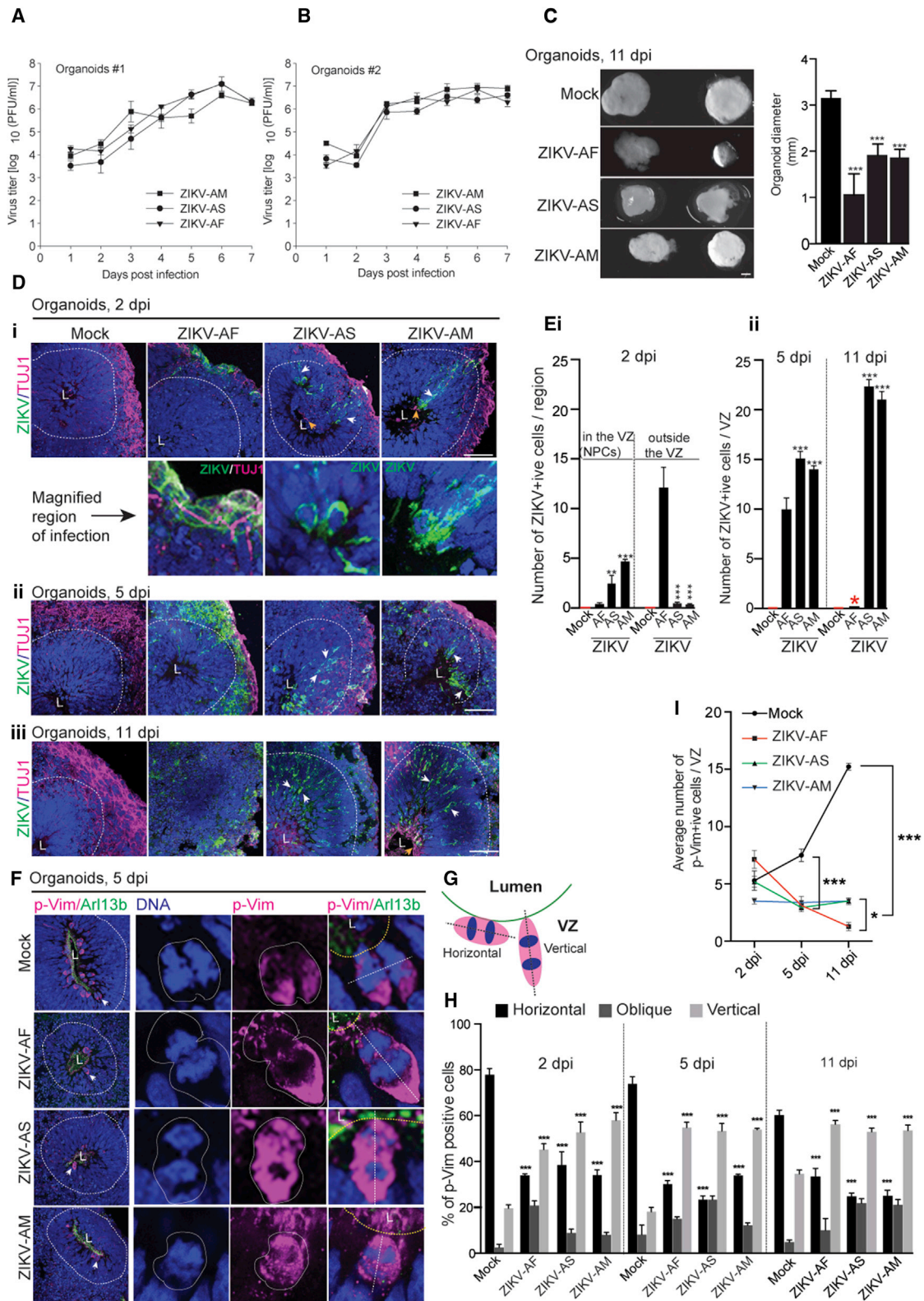
Figure 4. ZIKV-AS and AM Readily Target Apical Progenitors of Brain Organoids, Perturb Neurogenesis, and Display an Altered Division Plane of Mitotic Apical Progenitors

(A and B) ZIKV-AF/AS/AM virus titers in supernatants of brain organoids generated from two different iPSC lines. 9-day-old organoids were infected with 10^5 PFUs of ZIKV strains. Data are ± SEM; n = 3 independent experiments. Quantification details are listed in Table S2.

(legend continued on next page)

REFERENCES

Alcantara, D., and O'Driscoll, M. (2014). Congenital microcephaly. Am. J. Med. Genet. C. Semin. Med. Genet. *166C*, 124–139.

Bardy, C., van den Hurk, M., Eames, T., Marchand, C., Hernandez, R.V., Kellogg, M., Gorris, M., Galet, B., Palomares, V., Brown, J., et al. (2015). Neuronal medium that supports basic synaptic functions and activity of human neurons in vitro. Proc. Natl. Acad. Sci. USA *112*, E2725–E2734.

Baronti, C., Piorkowski, G., Charrel, R.N., Boubis, L., Leparc-Goffart, I., and de Lamballerie, X. (2014). Complete coding sequence of zika virus from a French Polynesia outbreak in 2013. Genome Announc. *2*, e00500–e00514.

Bazzi, H., and Anderson, K.V. (2014). Acentriolar mitosis activates a p53-dependent apoptosis pathway in the mouse embryo. Proc. Natl. Acad. Sci. USA *111*, E1491–E1500.

Bond, J., Roberts, E., Springell, K., Lizarraga, S.B., Scott, S., Higgins, J., Hampshire, D.J., Morrison, E.E., Leal, G.F., Silva, E.O., et al. (2005). A centrosomal mechanism involving CDK5RAP2 and CENPJ controls brain size. Nat. Genet. *37*, 353–355.

Brasil, P., Pereira, J.P., Jr., Moreira, M.E., Ribeiro Nogueira, R.M., Damasceno, L., Wakimoto, M., Rabello, R.S., Valderramos, S.G., Halai, U.A., Salles, T.S., et al. (2016). Zika Virus Infection in Pregnant Women in Rio de Janeiro - Preliminary Report. N. Engl. J. Med. *15*, 2321–2334.

Brault, J.B., Khou, C., Basset, J., Coquand, L., Fraisier, V., Frenkiel, M.P., Goud, B., Manuguerra, J.C., Pardigon, N., and Baffet, A.D. (2016). Comparative Analysis Between Flaviviruses Reveals Specific Neural Stem Cell Tropism for Zika Virus in the Mouse Developing Neocortex. EBioMedicine *10*, 71–76.

Calegari, F., and Huttner, W.B. (2003). An inhibition of cyclin-dependent kinases that lengthens, but does not arrest, neuroepithelial cell cycle induces premature neurogenesis. J. Cell Sci. *116*, 4947–4955.

Calegari, F., Haubensak, W., Haffner, C., and Huttner, W.B. (2005). Selective lengthening of the cell cycle in the neurogenic subpopulation of neural progenitor cells during mouse brain development. J. Neurosci. *25*, 6533–6538.

Calvet, G., Aguiar, R.S., Melo, A.S., Sampaio, S.A., de Filippis, I., Fabri, A., Araujo, E.S., de Sequeira, P.C., de Mendonça, M.C., de Oliveira, L., et al. (2016). Detection and sequencing of Zika virus from amniotic fluid of fetuses with microcephaly in Brazil: a case study. Lancet Infect. Dis. *16*, 653–660.

Cizmecioglu, O., Arnold, M., Bahtz, R., Settele, F., Ehret, L., Haselmann-Weiss, U., Antony, C., and Hoffmann, I. (2010). Cep152 acts as a scaffold for recruitment of Plk4 and CPAP to the centrosome. J. Cell Biol. *191*, 731–739.

Cugola, F.R., Fernandes, I.R., Russo, F.B., Freitas, B.C., Dias, J.L., Guimarães, K.P., Benazzato, C., Almeida, N., Pignatari, G.C., Romero, S., et al. (2016). The Brazilian Zika virus strain causes birth defects in experimental models. Nature *534*, 267–271.

D'Amelio, M., Cavallucci, V., and Cecconi, F. (2010). Neuronal caspase-3 signaling: not only cell death. Cell Death Differ. *17*, 1104–1114.

Dang, J., Tiwari, S.K., Lichinchi, G., Qin, Y., Patil, V.S., Eroshkin, A.M., and Rana, T.M. (2016). Zika Virus Depletes Neural Progenitors in Human Cerebral Organoids through Activation of the Innate Immune Receptor TLR3. Cell Stem Cell *19*, 258–265.

Dick, G.W., Kitchen, S.F., and Haddow, A.J. (1952). Zika virus. I. Isolations and serological specificity. Trans. R. Soc. Trop. Med. Hyg. *46*, 509–520.

Driggers, R.W., Ho, C.Y., Korhonen, E.M., Kuivanen, S., Jääskeläinen, A.J., Smura, T., Rosenberg, A., Hill, D.A., DeBiasi, R.L., Vezina, G., et al. (2016). Zika Virus Infection with Prolonged Maternal Viremia and Fetal Brain Abnormalities. N. Engl. J. Med. *374*, 2142–2151.

Fernando, P., Brunette, S., and Megeney, L.A. (2005). Neural stem cell differentiation is dependent upon endogenous caspase 3 activity. FASEB J. *19*, 1671–1673.

Gabriel, E., Wason, A., Ramani, A., Gooi, L.M., Keller, P., Pozniakovsky, A., Poser, I., Noack, F., Telugu, N.S., Calegari, F., et al. (2016). CPAP promotes timely cilium disassembly to maintain neural progenitor pool. EMBO J. *35*, 803–819.

Garcez, P.P., Diaz-Alonso, J., Crespo-Enriquez, I., Castro, D., Bell, D., and Guillemot, F. (2015). Cenpj/CPAP regulates progenitor divisions and neuronal migration in the cerebral cortex downstream of Ascl1. Nat. Commun. *6*, 6474.

Garcez, P.P., Loiola, E.C., Madeiro da Costa, R., Higa, L.M., Trindade, P., Delvecchio, R., Nascimento, J.M., Brindeiro, R., Tanuri, A., and Rehen, S.K. (2016). Zika virus impairs growth in human neurospheres and brain organoids. Science *352*, 816–818.

Götz, M., and Huttner, W.B. (2005). The cell biology of neurogenesis. Nat. Rev. Mol. Cell Biol. *6*, 777–788.

(C) Age-matched ZIKV-infected brain organoids are smaller than uninfected ones at 11 dpi. Scale bar, 0.5 mm. Data are ± SEM. ***p < 0.001, one-way ANOVA followed by Tukey's multiple comparison test. n = 3 independent experiments. Quantification details are listed in Table S2.

(D) Kinetics of ZIKV infection. ZIKV-AS/AM target apical progenitors of the VZ at various time points tested (i–iii). At 2 dpi, ZIKV-AF localizes at a region away from the VZ. See also Figures S2A and S2B. The dotted line borders the periphery of the VZ. The TUJ1-labeled area (magenta) suggests a primitive cortical plate (CP) (i). Magnified images of the region infected by ZIKV-AF (organoid surface) and ZIKV-AS/AM (VZ) are shown. White arrows mark ZIKV-AS/AM labeling the radial process of radial glial cells. Yellow arrows mark TUJ1-positive neurons (magenta) at the VZ of ZIKV-AM and AS-infected organoids, suggestive of premature neurogenesis. At 11 dpi, the architecture of the VZ is still observed in ZIKV-AS/AM-infected organoids (bottom right), whereas the cyto-architecture of VZ in ZIKV-AF-infected organoids is not recognized. L, lumen of the VZ. Scale bar, 50 μm. See also Figure S1C for electron-dense ZIKV particles in organoids.

(E) Average number of ZIKV-positive cells within and outside of the VZ at 2 dpi (i). Shown is the average number of ZIKV-positive cells per VZ at 5 and 11 dpi (ii). At 11 dpi, no VZ-like architecture is observed in ZIKV-AF-infected organoids (asterisk). Data are ± SEM. ***p < 0.001, **p < 0.01, one-way ANOVA. Comparisons were made between ZIKV-AF versus low-passage strains. More than 30 VZs of organoids generated from two iPSC lines were analyzed. A summary of quantification is given in Table S2.

(F) The division plane of mitotic radial glial cells relative to the lumen surface of the VZ is specified by phospho-vimentin staining. Mitotic cells in mock organoids are mostly horizontally oriented (0–30°). Arl13b (green, at low magnification) specifies the apical lumen surface of the VZ. Most of the radial glial cells of ZIKV-infected organoids are vertically oriented (60–90°). Yellow dotted lines at high magnification mark the apical side of the lumen, which is ciliated (Arl13b, green). The straight line shows axes of the division plane (right).

(G) Schematic providing vertical or horizontal orientation of the division plane of cells relative to the lumen.

(H) Percentages of division planes of mitotic radial glial cells in ZIKV-AF/AS/AM-infected organoids at 2, 5, and 11 dpi. n = 6 organoids from three different batches. n = 7 organoids from three different batches. Data are ± SEM. ***p < 0.001, two-way ANOVA.

(I) Progressive decline in phospho-vimentin-positive radial glial cells in ZIKV-infected organoids. Note the increasing numbers of mitotic radial glial cells in uninfected organoids. Error bars show mean ± SEM. ***p < 0.001 (infected versus control at 5 and 11 dpi) and mean ± SEM. *p < 0.05 (ZIKV-AF versus ZIKV-AS and ZIKV-AM at 11 dpi), ordinary two-way ANOVA; for mock six organoids from three different batches, and for each ZIKV strain, seven organoids from three different batches. Details are listed in Table S2.

Graser, S., Stierhof, Y.D., Lavoie, S.B., Gassner, O.S., Lamla, S., Le Clech, M., and Nigg, E.A. (2007). Cep164, a novel centriole appendage protein required for primary cilium formation. J. Cell Biol. *179*, 321–330.

Guernsey, D.L., Jiang, H., Hussin, J., Arnold, M., Bouyakdan, K., Perry, S., Babineau-Sturk, T., Beis, J., Dumas, N., Evans, S.C., et al. (2010). Mutations in centrosomal protein CEP152 in primary microcephaly families linked to MCPH4. Am. J. Hum. Genet. *87*, 40–51.

Hamel, R., Dejarnac, O., Wichit, S., Ekchariyawat, P., Neyret, A., Luplertlop, N., Perera-Lecoin, M., Surasombatpattana, P., Talignani, L., Thomas, F., et al. (2015). Biology of Zika Virus Infection in Human Skin Cells. J. Virol. *89*, 8880–8896.

Herz, J., Pardo, J., Kashkar, H., Schramm, M., Kuzmenkina, E., Bos, E., Wiegmann, K., Wallich, R., Peters, P.J., Herzig, S., et al. (2009). Acid sphingo-myelinase is a key regulator of cytotoxic granule secretion by primary T lymphocytes. Nat. Immunol. *10*, 761–768.

Hussain, M.S., Baig, S.M., Neumann, S., Nürnberg, G., Farooq, M., Ahmad, I., Alef, T., Hennies, H.C., Technau, M., Altmüller, J., et al. (2012). A truncating mutation of CEP135 causes primary microcephaly and disturbed centrosomal function. Am. J. Hum. Genet. *90*, 871–878.

Insolera, R., Bazzi, H., Shao, W., Anderson, K.V., and Shi, S.H. (2014). Cortical neurogenesis in the absence of centrioles. Nat. Neurosci. *17*, 1528–1535.

Kalay, E., Yigit, G., Aslan, Y., Brown, K.E., Pohl, E., Bicknell, L.S., Kayserili, H., Li, Y., Tüysüz, B., Nürnberg, G., et al. (2011). CEP152 is a genome maintenance protein disrupted in Seckel syndrome. Nat. Genet. *43*, 23–26.

Lancaster, M.A., Renner, M., Martin, C.A., Wenzel, D., Bicknell, L.S., Hurles, M.E., Homfray, T., Penninger, J.M., Jackson, A.P., and Knoblich, J.A. (2013). Cerebral organoids model human brain development and microcephaly. Nature *501*, 373–379.

Li, H., Saucedo-Cuevas, L., Regla-Nava, J.A., Chai, G., Sheets, N., Tang, W., Terskikh, A.V., Shresta, S., and Gleeson, J.G. (2016). Zika Virus Infects Neural Progenitors in the Adult Mouse Brain and Alters Proliferation. Cell Stem Cell *19*, 593–598.

Mariani, J., Coppola, G., Zhang, P., Abyzov, A., Provini, L., Tomasini, L., Amenduni, M., Szekely, A., Palejev, D., Wilson, M., et al. (2015). FOXG1-Dependent Dysregulation of GABA/Glutamate Neuron Differentiation in Autism Spectrum Disorders. Cell *162*, 375–390.

McLean, J.E., Wudzinska, A., Datan, E., Quaglino, D., and Zakeri, Z. (2011). Flavivirus NS4A-induced autophagy protects cells against death and enhances virus replication. J. Biol. Chem. *286*, 22147–22159.

Mlakar, J., Korva, M., Tul, N., Popović, M., Poljšak-Prijatelj, M., Mraz, J., Kolenc, M., Resman Rus, K., Vesnaver Vipotnik, T., Fabjan Vodušek, V., et al. (2016). Zika Virus Associated with Microcephaly. N. Engl. J. Med. *374*, 951–958.

Moya, N., Cutts, J., Gaasterland, T., Willert, K., and Brafman, D.A. (2014). Endogenous WNT signaling regulates hPSC-derived neural progenitor cell heterogeneity and specifies their regional identity. Stem Cell Reports *3*, 1015–1028.

Nowakowski, T.J., Pollen, A.A., Di Lullo, E., Sandoval-Espinosa, C., Bershteyn, M., and Kriegstein, A.R. (2016). Expression Analysis Highlights AXL as a Candidate Zika Virus Entry Receptor in Neural Stem Cells. Cell Stem Cell *18*, 591–596.

Onorati, M., Li, Z., Liu, F., Sousa, A.M., Nakagawa, N., Li, M., Dell'Anno, M.T., Gulden, F.O., Pochareddy, S., Tebbenkamp, A.T., et al. (2016). Zika Virus Disrupts Phospho-TBK1 Localization and Mitosis in Human Neuroepithelial Stem Cells and Radial Glia. Cell Rep. *16*, 2576–2592.

Paşca, A.M., Sloan, S.A., Clarke, L.E., Tian, Y., Makinson, C.D., Huber, N., Kim, C.H., Park, J.Y., O'Rourke, N.A., Nguyen, K.D., et al. (2015). Functional cortical neurons and astrocytes from human pluripotent stem cells in 3D culture. Nat. Methods *12*, 671–678.

Qian, X., Nguyen, H.N., Song, M.M., Hadiono, C., Ogden, S.C., Hammack, C., Yao, B., Hamersky, G.R., Jacob, F., Zhong, C., et al. (2016). Brain-Region-Specific Organoids Using Mini-bioreactors for Modeling ZIKV Exposure. Cell *165*, 1238–1254.

Rakic, P. (1995). A small step for the cell, a giant leap for mankind: a hypothesis of neocortical expansion during evolution. Trends Neurosci. *18*, 383–388.

Rauch, A., Thiel, C.T., Schindler, D., Wick, U., Crow, Y.J., Ekici, A.B., van Essen, A.J., Goecke, T.O., Al-Gazali, L., Chrzanowska, K.H., et al. (2008). Mutations in the pericentrin (PCNT) gene cause primordial dwarfism. Science *319*, 816–819.

Rubenstein, J.L.R., and Rakic, P. (2013). Patterning and cell type specification in the developing CNS and PNS, First Edition (Amsterdam, Boston: Elsevier/AP).

Schindelin, J., Arganda-Carreras, I., Frise, E., Kaynig, V., Longair, M., Pietzsch, T., Preibisch, S., Rueden, C., Saalfeld, S., Schmid, B., et al. (2012). Fiji: an open-source platform for biological-image analysis. Nat. Methods *9*, 676–682.

Tang, H., Hammack, C., Ogden, S.C., Wen, Z., Qian, X., Li, Y., Yao, B., Shin, J., Zhang, F., Lee, E.M., et al. (2016). Zika Virus Infects Human Cortical Neural Progenitors and Attenuates Their Growth. Cell Stem Cell *18*, 587–590.

Tapias, A., Zhou, Z.W., Shi, Y., Chong, Z., Wang, P., Groth, M., Platzer, M., Huttner, W., Herceg, Z., Yang, Y.G., and Wang, Z.Q. (2014). Trrap-dependent histone acetylation specifically regulates cell-cycle gene transcription to control neural progenitor fate decisions. Cell Stem Cell *14*, 632–643.

Ventura, C.V., Maia, M., Bravo-Filho, V., Góis, A.L., and Belfort, R., Jr. (2016). Zika virus in Brazil and macular atrophy in a child with microcephaly. Lancet *387*, 228.

Yingling, J., Youn, Y.H., Darling, D., Toyo-Oka, K., Pramparo, T., Hirotsune, S., and Wynshaw-Boris, A. (2008). Neuroepithelial stem cell proliferation requires LIS1 for precise spindle orientation and symmetric division. Cell *132*, 474–486.

Zheng, X., Gooi, L.M., Wason, A., Gabriel, E., Mehrjardi, N.Z., Yang, Q., Zhang, X., Debec, A., Basiri, M.L., Avidor-Reiss, T., et al. (2014). Conserved TCP domain of Sas-4/CPAP is essential for pericentriolar material tethering during centrosome biogenesis. Proc. Natl. Acad. Sci. USA *111*, E354–E363.

STAR★METHODS

KEY RESOURCES TABLE

REAGENT or RESOURCE	SOURCE	IDENTIFIER
Antibodies and Detection reagents		
ARL13B rabbit polyclonal antibody	Proteintech	17711-1-AP; RRID: AB_2060867
Axl (C89E7) Rabbit mAb	Cell Signaling	#8661; RRID: AB_11217435
Click-iT® EdU Alexa Fluor® 594 Imaging Kit (Molecular Probes)	Thermo Fisher Scientific	C10339
DeadEnd Fluorometric TUNEL system	Promega	G3250
Goat anti-Mouse IgG (H+L) Secondary Antibody, Alexa Fluor 488	Invitrogen	A-11001
Goat anti-Rabbit IgG (H+L) Secondary Antibody, Alexa Fluor 647	Invitrogen	A-21245; RRID: AB_141775
mouse anti-flavivirus group antigen monoclonal antibody	Millipore	D1-4G2-4-15
mouse anti-SOX2 [9-9-3]	Abcam	ab79351; RRID: AB_10710406
mouse monoclonal anti-CPAP		Gabriel et al., 2016
Nestin mouse monoclonal antibody (4D11)	Novus biologicals	NBP1-92717; RRID: AB_11020601
phospho-Vimentin (Ser55) mAb	MBL	D076-3S; RRID: AB_592962
rabbit anti-Cep152		Gabriel et al., 2016
rabbit anti-Cep164	Kind gift from Erich Nigg	
rabbit anti-Doublecortin	Synaptic Systems	326 003; RRID: AB_2620067
rabbit anti-MAP2	Proteintech	17490-1-AP; RRID: AB_2137880
rabbit anti-PAX6	Covance/Biolegend	clone poly19013; RRID: AB_2565003
Sox2 (D9B8N) Rabbit mAb	Cell Signaling	#23064
Chemicals, Peptides, and Recombinant Proteins		
Accutase solution	Sigma-Aldrich	A6964-100ML
ascorbic acid	Sigma-Aldrich	A4403
B-27 Supplement (50X), minus vitamin A	Thermo scientific	12587010
Brainphys	Stem cell technologies	#05790
cAMP	Sigma-Aldrich	A9501
DAPI	Sigma-Aldrich	32670
Dorsomorphin	Sigma-Aldrich	P5499
GDNF	Peprotech	450-10
Gelatin from cold water fish skin	Sigma-Aldrich	G7765-250ML
Insulin	Sigma-Aldrich	I3536-100MG
Laminin	Sigma-Aldrich	L2020
Leibovitz 15	Thermo scientific	11415064
Matrigel hESC-qualified matrix	Corning	354277
mTeSR1	Stem cell technologies	# 05850
N-2 Supplement (100X)	Thermo scientific	17502048
Neural Basal Medium	GIBCO	21103049
Neural induction medium (NIM)	Stem cell technologies	21103049
NT3	Sigma-Aldrich	SRP3128
Poly-L-lysine solution	Sigma-Aldrich	P8920-100ML
Poly-L-ornithine solution	Sigma-Aldrich	P4957
SB431542	Selleckchem.com	S1067
STEMdiff Neural Progenitor Medium	Stem cell technologies	# 05833
STEMdiff Neural rosette selection medium	Stem cell technologies	# 05832

REAGENT or RESOURCE	SOURCE	IDENTIFIER
Experimental Models: Cell Lines		
C6/36	ATCC	Aedes albopictus clone C6/36 (ATCC CRL-1660)
Human iPSC donor 1	Generated by Gabriel et al., 2016	iPSC from human BJ6 fibroblasts (Miltenyi, 130-096-726)
Human iPSC donor 2	WiCell	IMR-90
Vero cells	ATCC	Vero (ATCC CCL-81)
Experimental Models: Organisms/Strains		
LCMV, strain WE	Herz et al., 2009	LCMV-WE
ZIKV-AF (MR766)	ATCC	MR766 Zika virus (ATCC VR-84)
ZIKV-AM (FB-GWUH-2016)	Driggers et al., 2016	FB-GWUH-2016
ZIKV-AS (Zika-virus strain from French Polynesia)	European Virus Archive (EVA; Marseille, France; approved by Xavier de Lamballerie)	H/PF/2013
Software and Algorithms		
Adobe Photoshop CS6	Adobe	
Fiji win64 (ImageJ 1.47t)	Wayne Rasband, NIH, USA	Schindelin et al. (2012)
Prism		GraphPad Prism version 6.0d

CONTACT FOR REAGENT AND RESCOURCE SHARING

As Lead Contact, Jay Gopalakrishnan (CMMC, University of Cologne) is responsible for all reagent and resource requests. Please contact Jay Gopalakrishnan at jay.gopalakrishnan@uni-koeln.de with requests and inquiries.

EXPERIMENTAL MODEL AND SUBJECT DETAILS

ZIKV and LCMV-WE strains

Zika virus ZIKV-AS, strain H/PF/2013 from a French Polynesian outbreak 2013 (Baronti et al., 2014), was purchased from the European Virus Archive (EVA; Marseille, France; approved by Xavier de Lamballerie). ZIKV-AF (MR766, original) was purchased from ATCC and FB-GWUH-2016 (ZIKV-AM) was obtained from Dr. Vapalahti group (Dick et al., 1952; Driggers et al., 2016). Each Zika virus strain was propagated on Aedes albopictus C6/36 cells (from ATCC) in Leibovitz 15 (L-15) growth medium supplemented with 5% FCS at 28°C. Lymphocytic Choriomeningitis Virus (LCMV), strain WE, was propagated and titrated as plaque-forming units (PFU) on L929 (from ATCC) (Herz et al., 2009). Virus preparations have been handled under Biosafety Level 3 precautions, although only Biosafety Level 2 is recommended by WHO. Any handling with Zika virus and viral-infected cultures were performed in appropriately equipped laboratories by staff trained in the relevant technical and safety procedures. National guidelines on laboratory biosafety have been followed in all circumstances.

Human iPSCs

Two independent human iPSC lines were used. One iPSC line has been regenerated in our laboratory by reprogramming foreskin BJ6 fibroblasts. This iPSC line has been previously characterized in Gabriel et al. (2016). The second line is a commercially available IMR-90 from Wicell. Both lines were routinely cultured under feeder-free condition in mTeSR1 medium (Stem cell technologies) on Matrigel (Corning) coated tissue culture treated dishes. Medium was changed daily and iPSC were passaged enzyme-free with ReLSR reagent after 5 to 7 days when cells reached approx. 80% of confluency.

iPSC-derived NPCs, brain organoids and Neurons

NPCs, neurons and brain organoids used in this study were generated from above-mentioned two independent iPSC lines. NPCs were maintained in STEMdiff Neural Progenitor Medium (Stem cell technologies, USA) under non-differentiating conditions and sub-cultured for every 5 - 7 days. Human organoids from two different iPSC lines were cultured in spinner flasks containing medium mixture of DMEM/F12 and Neural Basal Medium (in 1:1 ratio), supplemented with 1:200 N2, 1:100 B27 w/o vitamin A, 1:100 L-glutamine, 0.05 mM MEM non-essential amino acids (NAA), 100 U/ml penicillin, 100 μg/ml streptomycin, 1.6 g/L insulin (Sigma-Aldrich) and 0.05 mM β-mercaptoethanol (all from Life Technologies if not stated) and supplemented with 0.5 μmol dorsomorphin (Sigma-Aldrich, USA) and 5 μM SB431542 (Selleckchem, USA). Differentiated cortical neurons from two different iPSC lines were maintained in a medium consisting of BrainPhys basal medium(Bardy et al., 2015) supplemented with 1x B27 (without vitamin A, Thermo scientific, USA), 1x N2 (Thermo scientific, USA), 20ng/ml BDNF (Peprotech, USA), 20ng/ml GDNF (Peprotech, USA), 20ng/ml NT3, 1 μM

cAMP (Sigma, USA) and 0.2 μM ascorbic acid (Sigma, USA). Fresh medium was added every 2-3 days. Neurons were grown on PLO/laminin coated dishes. All cell lines (iPSCs, NPCs, organoids and neurons) were tested and found free from mycoplasma contamination.

METHOD DETAILS

ZIKV counting
Virus titers were quantified by a plaque assay on Vero cells (from ATCC) adapted to the 96-well format (Hamel et al., 2015). Cells were plated at a density of 1.2×10^4 cells/well in 100μl DMEM, 5% FCS, on 96-well plates and incubated at 37°C, 5% CO_2 atmosphere. On the next day, 100μl of appropriate ten-fold dilutions (usually ranging from undiluted to 10^{-5}-fold diluted) of supernatants from infected cultures were added to each well. After incubation for 3 days, supernatants were discarded and the Vero cell layer was fixed and stained with 0.2% crystal violet, 11% vol formaldehyde, 2% vol ethanol, for 15 min, rinsed with water and dried, before virus plaques were counted at 4-fold magnification with an inverted microscope (Leica, Germany). Virus content of the supernatants was calculated as plaque forming units (PFU)/ml.

Virus infection
Number of ZIKV particles or PFU used to infect cells or organoids are given in respective figures and identical for all three ZIKV strains.
  Lymphocytic Choriomeningitis Virus (LCMV), strain WE, was propagated and titrated as plaque-forming units (PFU) on L929 (from ATCC). PFU values were converted into infectious units (IU) by multiplying PFU by 10(Herz et al., 2009). Organoids were infected with 10(5) PFU of either LCMV-WE or ZIKV-AF or treated with medium. Quantification details for organoid number are provided in Table S2.

Mock treatment
To prove that the effects observed were induced by ZIKV infection rather than by bioactive contaminants, for key experiments we included controls treated with (i) supernatants of non-infected C6/36 cells and (ii) UV-irradiated virus stocks. UV irradiation at a dose of 2000 J/m^2 was performed with a Hoefer UVC500 Ultraviolet Crosslinker as recommend by WHO guidelines (WHO Technical Report, Series No 924, 2004; p. 204).

Differentiation of iPSCs into NPCs
STEMdiff Neural Induction Medium (Stem cell technologies, USA) was used to differentiate iPSC lines into neural progenitor cells (NPCs). Five days later, the formed neurospheres were collected and cultured on poly-L-ornithine (PLO)-/laminin coated dishes. The medium was thereafter changed daily. 7 days later, the neural rosettes were selected using neural rosette selection medium (Stem cell technologies, USA) and re-cultured. NPCs were further maintained in STEMdiff Neural Progenitor Medium (Stem cell technologies, USA) under non-differentiating conditions and subcultured for every 5 - 7 days.

NPC culture and infection
NPCs were differentiated from two different donor iPSC lines and cultured as monolayer in *STEMdiff* Neural Induction Medium (Stem cell technologies, USA) on poly-L-ornithine (PLO)-/laminin coated glass coverslips in 24-TC well plates with a density of 2×10^4 cells per well at 37°C and 5% CO_2 atmosphere. Infection with ZIKV-AF, ZIKV-AS or ZIKV-AM followed one day after NPC seeding for 4 days (dpi 4) or 7 days (dpi 7) prior analysis.

Generation of brain organoids
Organoids were generated by dissociating human iPSCs at 80% confluency into single cells with 5 min of accutase (Sigma-Aldrich) treatment at 37°C. After centrifuge step of 1000 x g and 4 min, iPSCs were resuspended in neural induction medium (NIM, Stem cell technologies) and 10 μM Rock-Inhibitor at a concentration of $4.5*10^5$ cells per ml. Then, 100 μl of cell suspension was distributed into each well of a low-adherent 96-Well V-bottom plate, followed by careful centrifuge step at 500 x g for 3 min. Medium was changed half every day for the next 5 days. After 5 days of differentiation neurospheres were harvested and embedded in matrigel (Corning, USA) drops. Differentiation medium mixture of DMEM/F12 and Neural Basal Medium (in 1:1 ratio), supplemented with 1:200 N2, 1:100 B27 w/o vitamin A, 1:100 L-glutamine, 0.05 mM MEM non-essential amino acids (NAA), 100 U/ml penicillin, 100 μg/ml strep-tomycin, 1.6 g/L insulin (Sigma-Aldrich) and 0.05 mM β-mercaptoethanol (all from Life Technologies if not stated) was used to differ-entiate the matrigel embedded droplets in suspension culture in a 100 mm petridish. After four days of culturing embedded neuro-spheres in petridishes, neurospheres were transferred to spinner flasks (IBS, integra biosciences). The flasks contained the same differentiation medium supplemented with 0.5 μmol dorsomorphin (Sigma-Aldrich, USA) and 5 μM SB431542 (Selleckchem, USA).

Infection of brain organoids
For infection with ZIKV-AF, ZIKV-AS, ZIKV-AM, LCMV-WE strains and UV-treated supernatant (mock), 9 day old organoids were transferred from spinner flasks into low-adherent 12 wellplates. Per well one organoid in 2 mL differentiation medium was incubated as stationary suspension culture and treated. For quantification details please refer Table S2.

Neuronal differention of human NPCs

NPCs were differentiated into cortical neurons according to the methods described by Moya et al. (2014). In detail, coverslips were coated with poly-L-ornithine (PLO)-/laminin and the NPCs were seeded on the coverslips as a monolayer. 48 hr later, NPCs were switched to cortical neuronal differentiation medium consisting of BrainPhys basal medium(Bardy et al., 2015) supplemented with 1x B27 (without vitamin A, Thermo scientific, USA), 1x N2 (Thermo scientific, USA), 20ng/ml BDNF (Peprotech, USA), 20ng/ml GDNF (Peprotech, USA), 20ng/ml NT3, 1 μM cAMP (Sigma, USA) and 0.2 μM ascorbic acid (Sigma, USA). Fresh medium was added every 2-3 days.

Infection of neurons

Differentiated neurons were grown on PLO-/laminin-coated glass coverslips in 24-wellplate format and infected with ZIKV strains (MOI 1.0) 3 weeks after start of neuronal differention from two different donor-NPCs. At 6 dpi, neurons were fixed and analyzed for neuronal markers (MAP2, Tau, NeuN, DCX, TUJ1), intracellular ZIKV and apoptosis (TUNEL).

Fixation of NPCs and neurons

For immunofluorescent analysis, monolayer NPCs and neurons were fixed for 10 min. and 3D-organoids for 30 min. in 4% paraformaldehyde/PBS (Gabriel et al., 2016).

Fixation and cryosectioning of organoids

Organoids were incubated in 30% sucrose over night at 4°C, embedded in Tissue-Tek O.C.T. compound (Sakura, Netherlands) and cryofrozen at −80°C before sectioning into 20 μm thin slices using Cryostat Leica CM3050 S.

Permeabilization, antigen retrieval and blocking

NPCs and organoid sections were permeabilized with 0.5% Triton X-100 for 10 min. and blocked with 0.5% fish gelatin/PBS for 1 hr, both at room temperature. For SOX2 and PAX6 stainings, antigen retrieval treatment with repeated heating (microwave) in Sodium citrate buffer (10 mM Sodium citrate, 0.05% Tween 20, pH 6.0) was applied after permeabilization and prior to blocking.

Immunofluorescent staining

Fixed cells and organoids were stained for different antigens as follows: mouse anti-flavivirus (clone D1-4G2-4-15, 1:2000, MERCK Millipore, Germany), mouse anti-nestin 4D11 (1:100, Novus Biologicals, Cambridge, USA), mouse anti-SOX2 (1:50, abcam, UK), rabbit anti-SOX2 (1:50, Cell Signaling, US), rabbit anti-PAX6 (clone poly19013, Covance/Biolegend, US), mouse monoclonal anti-CPAP (1:25), rabbit anti-TUJ1 (1:100, Sigma Aldrich, USA), rabbit anti-Cep152 (1:1250), rabbit anti-PCNT (1:1000, ab4448, abcam, UK), rabbit anti-Arl13b (1:100, Proteintech, Manchester, UK), rabbit anti-Doublecortin (1:200, Synaptic Systems, Germany), rabbit anti-AXL (1:50, Cell Signaling, Danvers, MA, USA), rabbit anti-MAP2 (1:200, Proteintech, Rosemont, IL, USA), rabbit anti-Cep164 (1:1000, E. Nigg) either overnight at 4°C or 1 hr at room temperature. For secondary antibodies, Alexa Fluor Dyes conjugated either with goat/donkey anti-mouse or anti-rabbit (1:1000, molecular probes, Thermo Fisher, USA) were used. For DNA staining, DAPI at a concentration of 1 μg/ml (Sigma Aldrich, USA) was used and the coverslips were mounted using Mowiol (Carl Roth, Germany).

TUNEL assay

Apoptotic cells were detected by using DeadEnd Fluorometric TUNEL System (Promega, Madison, USA) according to manufacturer's protocol.

EdU pulse labeling assay

EdU pulse labeling of NPCs was performed using Click-iT® EdU Alexa Fluor® 594 Imaging Kit (Molecular Probes) according to manufacturer's protocol 24 hr prior to fixation. Detection of EdU positive cells was performed by using Leica DMI6000 B widefield microscope. Determination of cell proliferation was based on EdU positive cells versus total cells (DAPI).

Determination of division plane in aRGs

Organoid thin sections were stained for mitotic aRGs (anti-phospho vimentin), cilia (anti Arl13b) and nuclei (DAPI). VZs within the organoid sections were visualized with Leica SP8 confocal microscope, 63x oil objective and 1x digital zoom (to count total phospho-vimentin positive cells per VZ) or 2x digital zoom (to evaluate cell division plane orientation). Luminal margin was determined by Arl13b positive cilia fringe emerging from aRGs into the lumen. Determination of division plane in phospho-vimentin positive aRGs was based on orientation of nuclei from phospho-vimentin positive cells in anaphase toward the luminal margin by manually screening of single z stacks. Horizontal orientation was defined as cell division plane parallel (0° to 30°) to cilia fringe, oblique as division plane 30° to 60° toward cilia fringe and vertical as perpendicular (60° to 90°) to cilia fringe (Rubenstein and Rakic, 2013).

Transmission electron microscopy

NPCs were fixed in 2.5% glutaraldehyde in PBS overnight at 4°C. A mixture of 2.5% glutaraldehyde in PBS and 1.8% sucrose was used to fix the organoids. Fixation was carried out overnight at 4°C. Samples were rinsed in PBS, post-fixed with 1% osmium tetroxide for 1 hr at 4°C. After the fixation, the samples were further dehydrated in a graded ethanol series, and embedded in Epon-Araldite

resin. Reichert Ultracut E ultramicrotome was used to obtain the Ulrathin sections (50-80nm), further stained with uranyl acetate and lead citrate, and observed with a FEI Tecnai G2 Spirit 255 transmission electron microscope operating at 100 kV.

Immuno electron microscopy

For pre-embedding immunoelectron microscopy, cells were fixed with 4% paraformaldehyde (EM grade) in PBS followed by a treatement with Triton X-100 (0.1% in PBS, 10 min) for permeabilization. After rinsing in PBS, samples were incubated overnight with mouse anti-flavivirus (clone D1-4G2-4-15, 1:2000, MERCK Millipore, Germany) primary antibody at 4°C. After washing in PBS, cells were incubated at room temperature for 1 hr with 5 nm gold conjugate goat anti-mouse IgG (1:20; Ted Pella, Inc.). Samples were rinsed in PBS, fixed in 2.5% glutaraldehyde in PBS for 30 min at 4°C, post-fixed with 1% osmium tetroxide in PBS for 30 min at 4°C, dehydrated through a graded series of ethanol, embedded with a mixture of Epon-Araldite resin and polymerized at 60°C for 48 hr.

Image acquisition

The raw images were collected using Leica SP8 confocal system (Leica microsystems, Germany) and processed with help of Fiji win64 (ImageJ 1.47t) and Adobe Photoshop (Adobe Systems, USA) (Schindelin et al., 2012).

ZIKV protein sequence alignment

Genome sequences of H/PF/2013 Zika-virus strain from French Polynesia, African MR766 strain and the recent ZIKV_FB-GWUH-2016 isolate were obtained from GenBank (Accession numbers KJ776791.1, AY632535.2, KU870645, respectively). The ORF of the Polyprotein were translated, compared pairwise and aligned using the blastp algorithm.

QUANTIFICATION AND STATISTICAL ANALYSIS

Statistical analysis was performed using GraphPad Prism version 6.0d by employing either student's t- test (unpaired, two-tailed), ordinary One-Way or Ordinary Two-Way ANOVA, ANOVA tests were always followed by Tukey's multiple comparison. Error bars are always ± s. e. m. Significance means *$p < 0.05$, **$p < 0.01$ or ***$p < 0.001$. Importantly, n = number of batches, whereas batch is defined by one culture starting from thawing human iPSCs and differentiating them to NPCs, neurons or brain organoids. Quantification details for organoids are listed in Table S2. Intensity measurements of images were obtained using ImageJ software. Statistical calculations were based on the relative fluorescence units estimated by the ImageJ software.